Research Square

Preprints are preliminary reports that have not undergone peer review.
They should not be considered conclusive, used to inform clinical practice,
or referenced by the media as validated information.

Hydrocarbon Diffusion in Siliceous Chabazite: Uptake Experiments and DFT-Corrected Transition-State Modeling

Tomáš Volný
Academy of Sciences of the Czech Republic
Jakub Halamek
University of Pardubice
Yosra Gherib
University of Pardubice
Roman Bulánek
University of Pardubice
Ota Bludský
ota.bludsky@uochb.cas.cz

Academy of Sciences of the Czech Republic

Article

Keywords: diffusion, chabazite, zeolites, uptake kinetics, hydrocarbons, transition-state theory, force fields, DFT calculations

Posted Date: November 13th, 2026

DOI: https://doi.org/10.21203/rs.3.rs-11251213/v1

License: This work is licensed under a Creative Commons Attribution 4.0 International License.
Read Full License

Additional Declarations: Competing interest reported. R.B. is an Editorial Board Member of Scientific Reports. The other authors declare no competing interests.

Hydrocarbon Diffusion in Siliceous Chabazite: Uptake Experiments and DFT-Corrected Transition-State Modeling

Tomáš Volný [a, c], Jakub Halamek[b], Yosra Gherib[b], Roman Bulánek[b], Ota Bludský [a,*]

[a]Institute of Organic Chemistry and Biochemistry, Academy of Sciences of the Czech Republic, Flemingovo nám. 2, 162 10 Prague, Czech Republic

[b]Department of Physical Chemistry, Faculty of Chemical Technology, University of Pardubice, Studentská 573, 532 10 Pardubice, Czech Republic

[c]Department of Physical and Macromolecular Chemistry, Faculty of Science, Charles University, Hlavova 8, 128 40 Prague, Czech Republic

*Corresponding author: ota.bludsky@uochb.cas.cz

Keywords:

diffusion; chabazite; zeolites; uptake kinetics; hydrocarbons; transition-state theory; force fields; DFT calculations

Abstract

Slow diffusion in narrow-pore zeolites is highly sensitive to molecular size and framework flexibility, and quantitative prediction is further complicated by the strong force-field dependence of molecular simulations. Here, we investigate the diffusion of C_1–C_4 alkanes and alkenes in pure-silica chabazite by combining molecular simulations with volumetric uptake experiments on the same hydrocarbon set. Uptake kinetics provides an experimental benchmark for relative transport rates across the hydrocarbon series. Diffusion coefficients are computed using a transition-state-theory hopping model based on finite-temperature free-energy profiles from metadynamics, employing two distinct zeolite force fields to assess force-field sensitivity. A DFT-based QM–MM barrier correction refines the enthalpic component of the activation energy and reduces the observed force-field dependence. The corrected diffusion trends reproduce the uptake-derived transport ordering across the full hydrocarbon series, supporting the use of corrected transition-state theory combined with uptake measurements as a validation strategy for slow-diffusion models in narrow-pore zeolites.

1 Introduction

Diffusion of guest molecules is a key process governing the performance of microporous materials used in catalysis, adsorption, and gas separation.[1-6] In these applications, molecular transport through the pore network can become rate-limiting when molecular size approaches aperture size.[7] This situation is particularly pronounced in narrow-pore zeolites, where diffusion proceeds via activated hopping through pore windows and diffusion coefficients may be several orders of magnitude lower than those in wide-pore materials.[8-10] The strong sensitivity of transport rates to small differences in molecular size and shape can enable kinetic separation of molecules with similar dimensions, such as propane and propene.[11-14]

Determining intracrystalline diffusion coefficients in the slow-hopping regime of narrow-pore zeolites remains challenging.[15] Direct experimental techniques probe different length and time scales and do not necessarily yield the same transport quantity.[10] Quasielastic neutron scattering (QENS) is primarily sensitive to local self-motion on picosecond-to-nanosecond timescales[16], whereas pulsed-field-gradient nuclear magnetic resonance (PFG NMR) probes self-diffusion over substantially longer observation times and displacement scales[10]; transient single-crystal microimaging can provide transport diffusivities and surface permeabilities but requires suitable optical contrast and sufficiently large crystals.[17-21] Conventional molecular dynamics faces a complementary limitation because slow cage-to-cage hopping in confined space may produce too few transitions within feasible trajectories.[22] Moreover, in the activated regime, predicted hopping rates depend exponentially on the window-crossing free-energy barrier and are therefore highly sensitive to the intermolecular potential and the flexibility response of the framework.[23-27]

Macroscopic gravimetric and volumetric methods measure the time-dependent uptake of adsorbates following a change in gas pressure and have long been used to characterize adsorption kinetics in porous solids.[18, 28] Crystal-size series in 4A zeolite provide an early example of their application to testing an intracrystalline-diffusion interpretation.[29] For an isothermal Fickian process in particles of known geometry and size distribution, the transient fractional uptake can be related to the diffusional rate parameter (D/R^2), or equivalently to the characteristic diffusion time (R^2/D); for spherical particles, the leading uptake term in the low-uptake limit is linear in $\sqrt{t}$.[28, 30] Identification of the fitted coefficient as an intrinsic intracrystalline transport diffusivity, however, requires the instrumental response to be substantially faster than the uptake process and external gas-phase and interparticle transport limitations, heat-transfer effects, and external surface barriers to be negligible.[28, 31] In general, the fitted coefficient represents an apparent diffusivity that reflects contributions from multiple transport processes and depends on the assumed diffusion length and particle-size distribution. Surface barriers can, for example, cause the apparent uptake diffusivity to depend strongly on crystal size even when the intrinsic intracrystalline diffusivity is essentially independent of crystal size.[32]

Analysis of the uptake curves yields apparent macroscopic transport diffusivities, whereas the simulations provide self-diffusion coefficients in the zero-loading limit; quantitative comparison is therefore most reliable at sufficiently low experimental loadings. The simulations can be evaluated primarily against the relative ordering of hydrocarbon uptake rates, while quantitative agreement between uptake-derived and simulated diffusivities should be interpreted with caution.

In this work, we combine volumetric uptake experiments and molecular simulations to evaluate slow hydrocarbon transport in pure-silica chabazite (Si-CHA). The uptake curves establish an experimental ranking of C_1–C_4 hydrocarbons, whereas the simulations provide self-diffusion

coefficients derived from finite-temperature free-energy profiles. We apply a density-functional theory (DFT)-based correction to the force-field barriers to test whether the self-diffusion coefficients predicted by two independent force fields converge after correction and whether the corrected simulations reproduce the experimentally observed uptake ordering. We show that the correction brings the results from the two force fields into close agreement across the full hydrocarbon series, that the corrected diffusion ordering reproduces the experimental uptake trends, and that static 0 K barriers alone are insufficient to capture the experimental ordering, underscoring the importance of finite-temperature and entropic contributions to slow diffusion in narrow-pore zeolites.

2 Methods

Experimental

Synthesis and characterization

A single Si-CHA sample was employed for all experiments. Si-CHA was synthesized hydrothermally using N,N,N-trimethyl-1-adamantylammonium hydroxide (TMAdaOH) as the OSDA, as described in literature[33, 34]. The final gel composition was: 1 SiO_2: 0.75 TMAdaOH: 0.75 HF: 4 H_2O. The procedure itself consisted of adding 19.7 g of a 25 wt.% TMAdaOH solution (CymitQuimica) over 6.5 g of tetraethyl orthosilicate (Merck). The resulting mixture was stirred until complete evaporation of the ethanol and excess water, achieving a final H_2O/SiO_2 molar ratio of 4.0. Subsequently, 1.17 g of aqueous HF (40 wt.%) (Merck) was added, and the synthesis gel was homogenized manually before being transferred into a 45 mL Teflon-lined stainless-steel autoclave. The crystallization process was conducted at 423 K for 5 days and 14 h. The resulting solid was thoroughly washed with redistilled water, dried, and then calcined at 853 K for 8 h to remove the organic template.

The synthesized sample underwent characterization using a set of conventional techniques (PXRD, SEM, N_2 adsorption/desorption isotherm measurement) to confirm the structure and purity and to determine the textural properties, such as the micropore volume and crystal size. The diffractogram was obtained on a tabletop Rigaku MiniFlex 600 device using CuKα radiation and Debye-Scherrer geometry, the SEM images were recorded using a tabletop Hitachi TM4000Plus II instrument, and the N_2 adsorption isotherm was measured on a Micromeritics ASAP 2020 Plus Physisorption volumetric device (the same device that was subsequently used for the uptake curve measurements). Prior to the adsorption isotherm measurement, the sample was degassed under dynamic vacuum at 523 K for 6 hours. The t-plot method was employed to determine the micropore volume and the external surface area of the sample (using Harkins-Jura thickness curve equation). Further characterization details are provided in the Supplementary Information.

Hydrocarbon mass transport measurements

The hydrocarbon mass transport evaluation was performed on a commercial volumetric ASAP 2020 Plus Physisorption instrument (Micromeritics, United States), employing the ROA (“rate of adsorption”) plugin. The experiment monitored the pressure change (for up to 100 000 s) upon dosing a controlled quantity of the hydrocarbon gas into the evacuated sample tube. All experiments were performed at 303.15 K (controlled by Peltier thermostats with Pt sensors – temperature control accuracy ± 0.1 K), and they were performed on a single batch of the as-

obtained powder sample (~80 mg). Before each uptake-curve measurement, the sample underwent regeneration under dynamic vacuum at 473 K (depending on the last measured gas, the duration of the treatment varied from 1 to 33 hours, to ensure the full activation of the material). The uptake-curve measurement methodology is described in greater detail in the Supplementary Information.

The uptake curves were quantitatively evaluated by employing the short-time √t-law, valid for the low-uptake limit of the measured uptake curve (according to the recommendations by Kärger et al.[30]):

$$\gamma(t) = \frac{m(t)}{m(\infty)} \approx 6\sqrt{\frac{D}{R^2\pi}}\sqrt{t} \qquad (1)$$

where $\gamma(t)$ is the normalized gas uptake at t, $m(t)$ is the gas uptake at t, $m(\infty)$ is the equilibrium gas uptake, D is the diffusion coefficient, and R is the effective radius of the particle (approximately given by $R = 3\,V/A$ of a given particle, see Supplementary Information). The evaluation consisted of determining the initial slopes of the $m(t)/m(\infty) = f(\sqrt{t})$ curves. When evaluating the uptake curves of the gases which did not fully equilibrate within the recorded period, the limiting value determined for a faster isomer was employed (i.e., the equilibrium uptake of propene was employed when calculating the propane diffusivity, and the equilibrium uptake of (E)-but-2-ene was employed when calculating the diffusivity of the slow C_4 hydrocarbons).

This law was originally derived for isothermal diffusion into a spherical particle. The low-uptake √t approximation was used as a practical estimate because the crystals show a relatively narrow size distribution and approximately isotropic rhombohedral morphology (Supplementary Fig. S3). In addition, CHA has a three-dimensional homogeneous pore system, and weak adsorption combined with tight temperature control should reduce heat-transfer artifacts, particularly for the faster adsorbates.

Computational details

Diffusion was studied for a series of C_1–C_4 alkanes and alkenes in Si-CHA, selected as a model narrow-pore zeolite. CHA consists of cages interconnected by 8-membered ring (8MR) windows, making it well-suited for isolating diffusion across pore apertures.

Two distinct force fields were used to describe the zeolite framework to assess the sensitivity of diffusion predictions to framework flexibility:

- Sanders–Leslie–Catlow (SLC) force field, a polarizable model employing a core-shell description for oxygen atoms, harmonic O-Si-O angle terms, and nonbonded interactions described by Buckingham potentials.[35]
- Interface force field (iFF), a non-polarizable model with explicit harmonic Si-O bonds and angular terms (Si-O-Si and O-Si-O), and nonbonded interactions represented by a 12-6 Lennard-Jones potential with long-range tail corrections.[36]

Hydrocarbons were modeled using the united-atom TraPPE-UA force field, with bonded and nonbonded parameters taken from the original TraPPE parametrization.[37, 38] Hydrocarbon-zeolite interactions were described using TraPPE-zeo cross-interaction parameters.[39] All force-field molecular mechanics simulations were performed using LAMMPS.[40]

Electronic structure calculations were carried out using density functional theory as implemented in VASP.[41] Projector augmented-wave pseudopotentials were used with an energy cutoff of 400 eV.[42] Exchange-correlation effects were treated using the PBEsol functional augmented by Grimme's D2 dispersion correction.[43, 44] Γ-point sampling was sufficient due to the large simulation cells employed.

Initial chabazite structures were taken from the International Zeolite Association database.[45] Framework geometries were optimized at 0 K using both force fields with full cell relaxation. Symmetry analysis confirmed preservation of the rhombohedral CHA structure. For DFT calculations, previously optimized cell parameters were employed.[23] For finite-temperature simulations, a Niggli-reduced CHA unit cell was constructed and doubled along the diffusion direction to simplify the definition of the collective variable. The framework was equilibrated at various temperatures (250–500 K in 50 K increments) using a sequential NVT (0.5 ns) and NpT (5 ns) protocol at 1 atm. The equilibrated lattice parameters were averaged over the production trajectories after discarding the first 5% and were used for subsequent free-energy calculations.

Free energy surfaces governing diffusion were computed using well-tempered metadynamics as implemented in the PLUMED package interfaced with LAMMPS.[46] The collective variable (CV) was defined as the projection of the center-of-mass coordinate of the hydrocarbon molecule along the lattice vector corresponding to the diffusion path.

Following initial equilibration in the NVT ensemble, metadynamics simulations were performed using Nosé–Hoover chain thermostats. Biasing parameters (Gaussian height, width, and bias factor) were chosen based on preliminary simulations to ensure efficient barrier sampling and convergence. Free energy profiles were reconstructed from the accumulated bias using the PLUMED sum_hills utility. Three independent metadynamics simulations were performed for each probe molecule at each temperature. Since the doubled unit cell contains two barriers, each of which can be overcome in two directions, each probe–temperature combination results in 12 diffusion coefficients. The resulting diffusion coefficients were weight-averaged.

Diffusion was modeled as a sequence of activated hops between adjacent cages using the Bennett–Chandler formulation of transition state theory (TST).[24] The direction-specific hopping rate constants were calculated from the free energy profiles obtained from metadynamics as

$$k_{A\to B}^{\mathrm{TST}} = \sqrt{\frac{k_B\,T}{2\,\pi\,m}} \cdot \frac{\mathrm{e}^{-F(\xi^*)/(k_B\,T)}}{\int_{\mathrm{cage\ A}} \mathrm{e}^{-F(\xi)/(k_B\,T)}\,\mathrm{d}\xi}, \tag{2}$$

where k is the hopping rate, m is the mass of the molecule, F is the free energy, and ξ is the collective variable. The transition state is denoted by an asterisk. Preliminary calculations indicated recrossing corrections corresponding to a transmission coefficient of approximately 0.6 to 1.0 – a minor multiplicative correction that is negligible relative to the orders-of-magnitude variations in diffusion coefficient that are the focus of this study.

Subsequently, the self-diffusion coefficients were calculated as

$$D_{A\to B} = k_{A\to B}\,\lambda^2, \tag{3}$$

where λ is the cage-to-cage distance along the diffusion path.

Diffusion coefficients were evaluated at multiple temperatures and fitted to the Arrhenius equation. The results from both force fields were fitted jointly to obtain a single pre-exponential factor with different apparent activation energies. To address limitations of force-field free energy

barriers, a QM–MM correction scheme was applied.[15] The apparent activation energies were corrected by adding the difference between DFT and force-field potential-energy barriers at 0 K. Potential-energy barriers were calculated using the climbing-image nudged elastic band (CI-NEB) method.[47] For force-field calculations, 12 interpolated images were employed; for DFT, a reduced number of images was used due to computational cost. To locate the force-field low-energy adsorption minima, 1000 random initial structures were generated through random rotation and translation of the molecule within the pre-optimized framework. For DFT, 25 random initial structures were generated in the same way.

3 Results and Discussion

An experimental benchmark for mass transport of all C_1–C_4 alkanes and monoalkenes in Si-CHA was established using uptake kinetics and low-uptake $\sqrt{t}$ analysis. The apparent uptake rate decreases in the following order: methane >> ethene > ethane >> (E)-but-2-ene > propene >> but-1-ene > butane > propane > (Z)-but-2-ene >> isobutene ≈ isobutane. The hydrocarbon uptake curves are presented in Figure 1. All studied gases except isobutane and isobutene showed measurable uptake with a characteristic concave-shaped curve, whereas the branched C_4 hydrocarbons adsorbed only negligibly, consistent with limited access to the micropores. The initial uptake slope varies strongly across the hydrocarbon series.

The fastest uptake is observed for methane, ethane, and ethene. In the case of methane, the uptake is essentially instantaneous, whereas for ethane and ethene, less than two minutes suffice for reaching almost full uptake equilibrium. Propene and (E)-but-2-ene have been found to have roughly similar uptake rates (in both cases, full uptake is achieved within several hours), with the (E)-but-2-ene being slightly faster. The remaining gases (propane, butane, but-1-ene, and (Z)-but-2-ene) have all reached only relatively low uptakes within the recorded 100 000 seconds – the equilibration would thus likely require weeks.

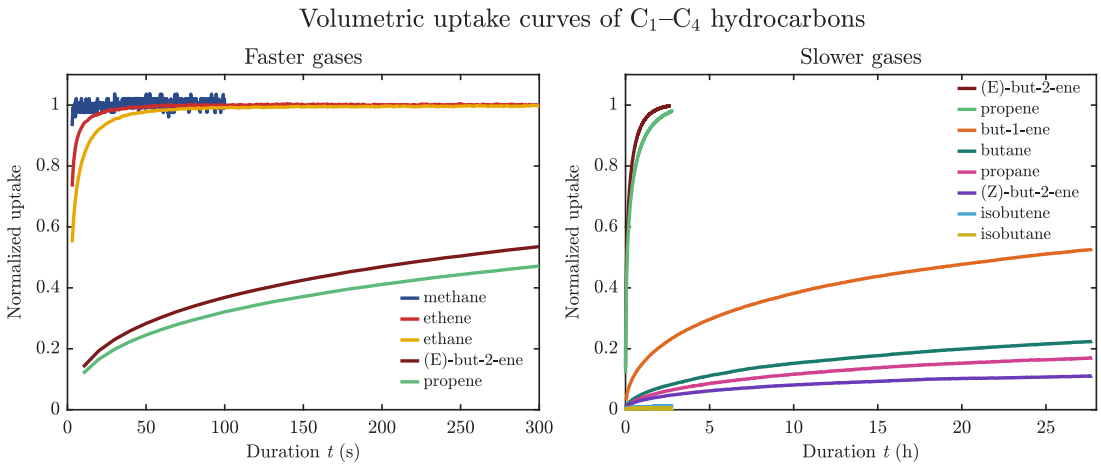


Figure 1: Normalized hydrocarbon uptake curves on Si-CHA at 303.15 K, (left) uptake curves of faster diffusing hydrocarbons, (right) uptake curves of slower diffusing hydrocarbons

To quantify the observed uptake behavior, the short-time $\sqrt{t}$-law introduced above was applied to the initial, low-uptake portion of each curve. The resulting linear fits are shown in Figure 2, with the fastest-equilibrating hydrocarbons (ethane, ethene, propene, and (E)-but-2-ene) plotted on the short timescale over which they approach uptake equilibrium, and the slower species (propane, butane, but-1-ene, and (Z)-but-2-ene) plotted on the extended timescale needed to

resolve their much smaller initial slopes. Methane was excluded from this analysis: its uptake occurs on a timescale comparable to the gas expansion into the measurement volume itself, so no linear fit could be reliably isolated for this gas.

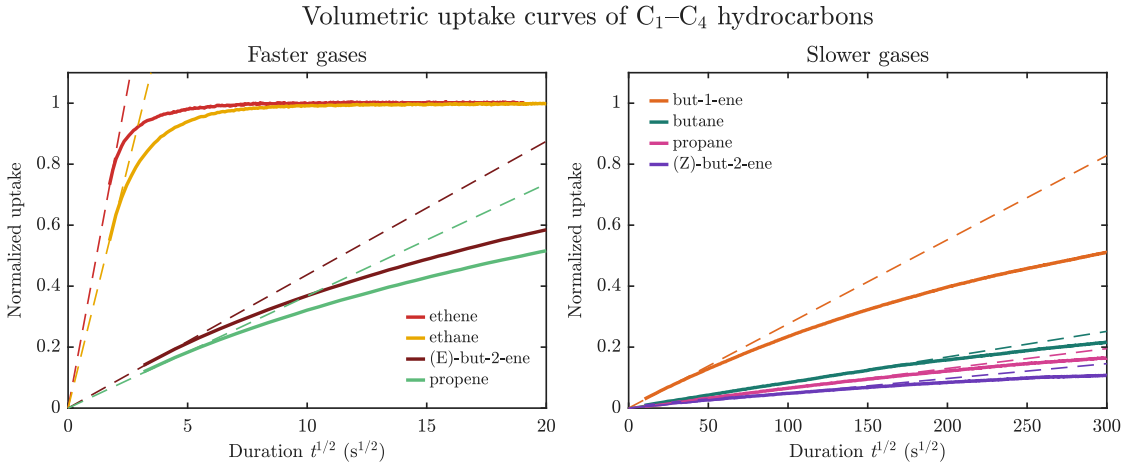


Figure 2: Short-time √t analysis of normalized volumetric uptake curves.

The resulting apparent diffusion coefficients are summarized in Table 1, both as the directly fitted parameter D/R^2 and as the diffusion coefficient D itself, after adopting an effective particle radius R = 8 μm (corresponding to an effective diameter of 16 μm for the almost cubic crystals studied here). As discussed above, these are apparent transport diffusivities rather than intrinsic self-diffusion coefficients, and their absolute magnitude carries the geometric uncertainty inherent in the assumed particle shape and size. Even so, the resulting ranking of hydrocarbon mobility is the central experimental result of this section and forms the benchmark against which the computed diffusion coefficients are evaluated.

Table 1: The calculated values of uptake-derived diffusivities of the investigated hydrocarbons in Si-CHA

	ethane	Ethene	propene	propane
D/R^2 (s^{-1})	8.78E-03	1.54E-02	1.18E-04	3.69E-08
D (m^2s^{-1})	5.62E-13	9.85E-13	7.55E-15	2.36E-18
	butane	but-1-ene	(E)-but-2-ene	(Z)-but-2-ene
D/R^2 (s^{-1})	6.14E-08	6.65E-07	1.67E-04	2.06E-08
D (m^2s^{-1})	3.93E-18	4.25E-17	1.07E-14	1.32E-18

To interpret the uptake-derived transport trends and evaluate the reliability of theoretical predictions in the slow-diffusion regime, diffusion coefficients were computed for the same series of hydrocarbons. Because diffusion across 8MR windows is highly sensitive to the description of host–guest interactions and framework flexibility, force-field dependence was assessed by employing two structurally distinct zeolite force fields (iFF and SLC) and using DFT-based barriers as the higher-level reference required for the QM–MM correction.[8, 48]

The computational analysis is organized in two steps: (i) quantifying barrier energetics via 0 K CI-NEB calculations and finite-temperature TST diffusion coefficients from metadynamics free energy profiles, and (ii) applying the QM–MM correction to test whether the force-field predictions converge after correction and reproduce the experimentally observed diffusion ordering.

CI-NEB calculations characterize the minimum-energy pathway for cage-to-cage hopping on the potential-energy surface. The corresponding 0 K potential-energy barriers for passage through the 8MR window were calculated using iFF and SLC and compared with the DFT barriers (Figure 3). Across the hydrocarbon series, iFF predicts systematically larger barriers than SLC. Relative to DFT, SLC tends to underestimate barriers, whereas iFF tends to overestimate them; the largest deviations occur for the slowest-diffusing molecules in the experimental ranking. Each barrier is derived from the change in the total potential energy of the guest–framework system and therefore includes contributions from changes in host–guest interactions and framework deformation. Structural changes of the 8MR window and the corresponding framework deformation energies along the hopping pathway are discussed in the Supplementary Information.

Barrier ordering among the heavier hydrocarbons depends strongly on the computational method. iFF predicts nearly identical barriers for but-1-ene, butane, and propane, whereas SLC differentiates among these molecules. DFT identifies butane as having the lowest barrier and propane as the highest within this subset. For (Z)-but-2-ene, both force fields predict substantially higher barriers than DFT, for which the barrier is close to that of butane. Agreement among the methods does not necessarily imply agreement with experiment: all three methods predict a higher barrier for methane than for ethene, despite the much faster experimental uptake of methane. Overall, the 0 K potential-energy barriers exhibit substantial method dependence and do not reproduce the experimental uptake trends. They are therefore insufficient on their own to predict the uptake-derived ordering of diffusion coefficients.

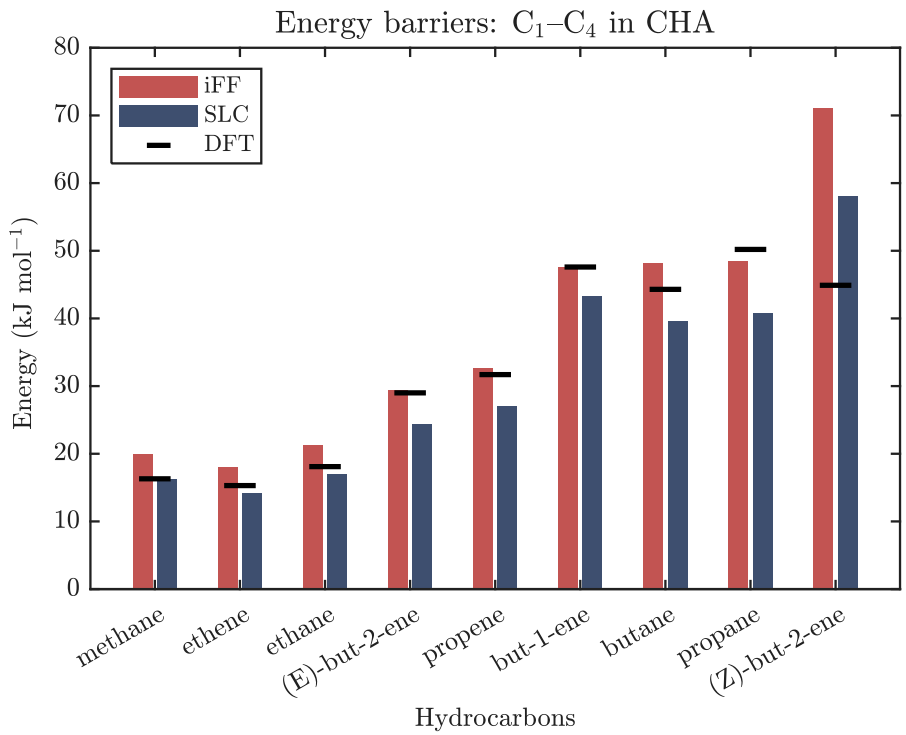


Figure 3: CI-NEB potential-energy barriers (kJ mol^{-1}) for C_1–C_4 hydrocarbons in Si-CHA at 0 K using different methods – iFF in red bars, SLC in blue bars, DFT in black markers. Hydrocarbons are ordered by decreasing experimental uptake rate.

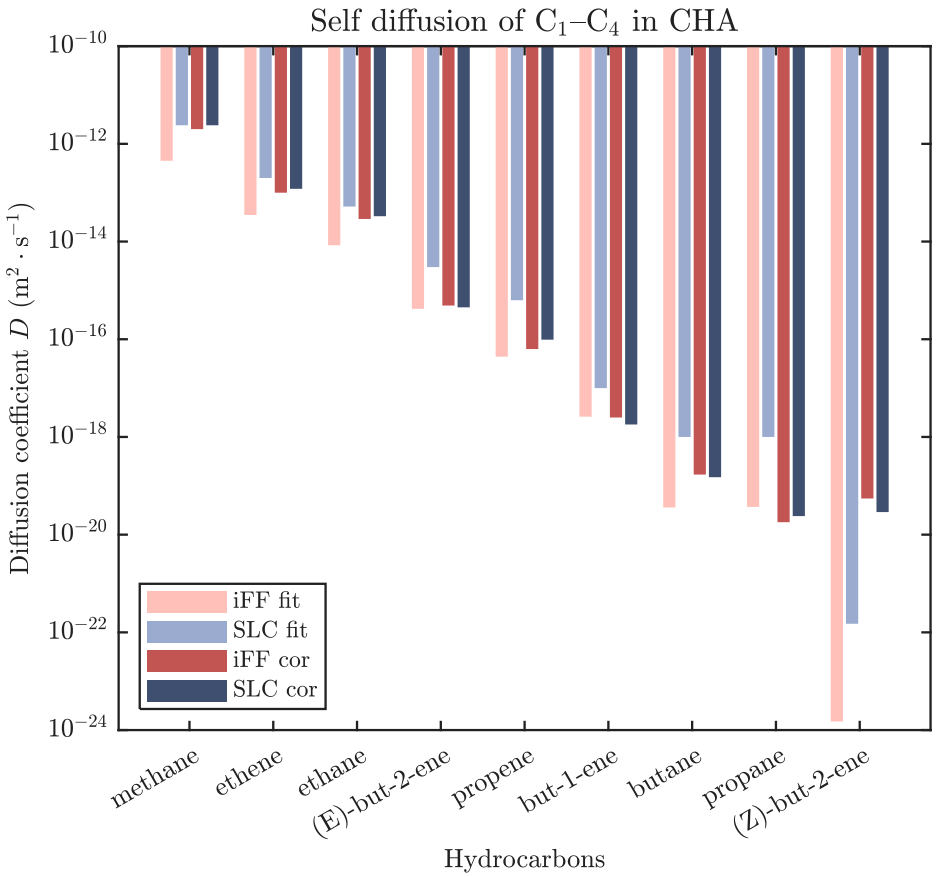


Figure 4: Calculated self-diffusion coefficients for C_1–C_4 hydrocarbons in Si-CHA at 300 K: values obtained from Arrhenius fit (light) and QM–MM correction scheme (dark) for iFF and SLC force fields, plotted on a base-10 logarithmic vertical axis. Hydrocarbons are ordered by decreasing experimental uptake rate.

The uncorrected diffusion coefficients were computed from metadynamics free-energy profiles using the TST hopping model described in the Methods section. The diffusion coefficients obtained at six temperatures between 250 and 500 K follow Arrhenius behavior within the statistical uncertainty of the simulations, although the SLC data show greater scatter around the fits than the iFF data. The iFF and SLC datasets were fitted jointly using a common pre-exponential factor and separate apparent activation energies. The apparent activation energies obtained with iFF are 4–12 kJ mol^{-1} higher than the corresponding SLC values, consistent with the systematically higher free-energy barriers predicted by iFF. The Arrhenius fits were then evaluated at 300 K. Figure 4 compares these diffusion coefficients with their QM–MM-corrected counterparts, with the hydrocarbons arranged in order of decreasing experimental uptake rate.

At 300 K, the computed diffusion coefficients span about ten orders of magnitude. Methane, ethene, and ethane exhibit the highest diffusion coefficients, whereas propane, butane, and (Z)-but-2-ene are among the slowest-diffusing molecules. This wide range illustrates the strong sensitivity of diffusion in Si-CHA to molecular size and shape.

The primary test of the QM–MM correction is whether it brings the diffusion coefficients predicted by iFF and SLC into agreement. The differences between the uncorrected TST diffusion coefficients (Figure 4) are consistent with the systematic differences in the 0 K CI-NEB barriers (Figure 3): relative to DFT, iFF generally predicts higher barriers, whereas SLC generally predicts lower barriers. The correction reduces the force-field dependence across the entire series and

makes the predicted diffusion ranking consistent between the two force fields. The largest corrections occur for the slowest-diffusing molecules, particularly (Z)-but-2-ene. Its uncorrected diffusion coefficients differ by more than two orders of magnitude between the force fields and are noticeably lower than those of propane, although the uptake-derived diffusivities of the two molecules are comparable. The correction increases the iFF and SLC diffusion coefficients of (Z)-but-2-ene by approximately four and two orders of magnitude, respectively, bringing them close to those of propane. For propane and butane, the correction likewise brings the iFF and SLC results into close agreement and improves the predicted ordering relative to experiment. The effect is more moderate for the smaller molecules, but it still reduces the differences between the force fields. Overall, the corrected iFF and SLC diffusion coefficients agree within one order of magnitude for every investigated hydrocarbon and differ substantially less than the uncorrected values. Thus, using the DFT–force-field differences in the 0 K potential-energy barriers to correct the apparent activation energies while retaining the entropic contributions from molecular-mechanics sampling largely removes the force-field dependence.

The second validation of the QM–MM approach is based on a comparison between the corrected diffusion coefficients and the experimental uptake-rate ordering. Uptake kinetics provide a robust relative transport ranking under controlled conditions, even when absolute diffusion coefficients are uncertain because of model assumptions (e.g., particle geometry) and possible contributions from non-intracrystalline resistances.

Figure 5 shows that the corrected diffusion coefficients reproduce the experimental uptake-rate ordering across all studied hydrocarbons, supporting the conclusion that the corrected theoretical framework captures the dominant factors controlling slow diffusion in Si-CHA. They also distinguish among the linear C_4 alkene isomers, consistent with their different equilibration times in the uptake curves. Quantitatively, the calculated diffusion coefficients are systematically approximately 1.5 orders of magnitude lower than the uptake-derived effective diffusivities across the entire dataset, suggesting that the discrepancy is not molecule-specific.

A systematic difference between the calculated and uptake-derived diffusion coefficients is not unexpected, as the simulations use an idealized molecular model, whereas uptake experiments probe real crystals and their analysis relies on geometrical assumptions. The uptake-derived diffusivity scales with R^2, where R is the assumed effective diffusion length; reducing R from 8 to 2 μm would lower the uptake-derived diffusivities by a factor of 16 and substantially reduce the observed offset. The offset may also reflect the conceptual difference between simulated self-diffusion coefficients and apparent transport diffusivities derived from uptake measurements, which coincide only in the dilute-loading limit. Framework defects, indicated by internal silanol bands in the FTIR spectra, may provide an additional source of systematic deviation.[49]

Beyond the experimental uncertainties discussed above, two limitations of the computational comparison should be noted. The QM–MM correction applies the differences between DFT and force-field 0 K CI-NEB barriers to apparent activation energies derived from finite-temperature sampling, assuming that these barrier differences are only weakly temperature-dependent over the investigated range. In addition, the simulations describe a defined cage-to-cage pathway in an idealized crystal, whereas uptake experiments average transport over real crystals and may include contributions beyond intracrystalline diffusion.

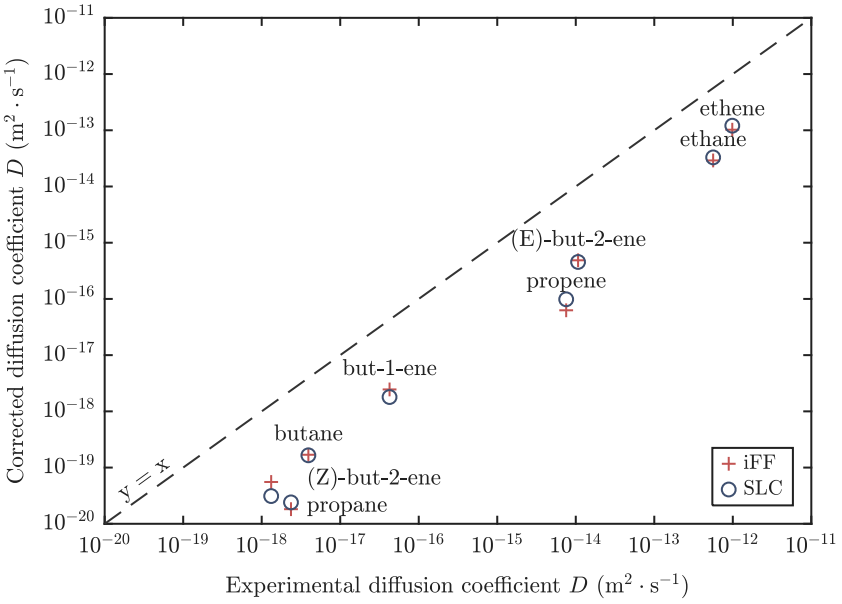


Figure 5: Correlation between uptake-derived diffusion coefficients and corrected simulated diffusion coefficients at 300 K. Crosses and circles show corrected iFF and SLC values, respectively. Both axes use base-10 logarithmic scaling.

The same correction concept can also be used to test models outside the classical force-field family. Machine-learning interatomic potentials can make long-time simulations closer to electronic-structure accuracy, but their reliability near diffusion transition states still requires validation. As an exploratory extension, the correction scheme was also tested for methane using UMA, a universal machine-learning interatomic potential.[50] Further results are provided in the Supplementary Information.

The present study focuses on a well-defined benchmark set for which both simulation and uptake experimental comparisons are meaningful. However, some hydrocarbons were excluded from the study. Methane was omitted from the experimental analysis because its faster diffusion takes place concurrently with the gas expansion into the chamber and it is therefore impossible to get any estimate. Branched C_4 hydrocarbons (isobutane and isobutene) exhibit negligible adsorption experimentally and extremely small self-diffusion coefficients in preliminary computations (the order of 10^{-52} and 10^{-44} m^2 s^{-1}, respectively), indicating diffusion far beyond experimentally accessible timescales and outside the practical resolution of the present computational protocol.

4 Conclusion

This work benchmarked a DFT-corrected transition-state framework for slow hydrocarbon diffusion against volumetric uptake kinetics – a widely accessible experimental technique – across a series of eleven C_1–C_4 alkanes and alkenes in pure-silica chabazite. Uptake measurements alone established a relative transport ordering spanning roughly six orders of magnitude. Metadynamics-based TST calculations likewise spanned many orders of magnitude but showed strong force-field dependence before correction. A DFT-based QM–MM correction of the enthalpic barrier component removed most of this dependence, bringing the iFF and SLC diffusion coefficients into close agreement for every modeled hydrocarbon.

After correction, the computed diffusion ordering reproduces the uptake-derived ordering, including the distinction among the linear C_4 alkene isomers, demonstrating that a comparatively simple experimental technique can meaningfully validate a substantially more demanding theoretical framework, at least at the level of relative transport rates. Absolute values remain systematically lower in the simulations by roughly 1.5 orders of magnitude, an offset that is not molecule-specific and likely reflects the assumed effective diffusion length, the difference between self- and transport diffusivities, and framework defects. Static 0 K CI-NEB barriers alone, by contrast, do not reproduce the experimental ordering, showing that finite-temperature and entropic contributions remain essential in this regime. The same correction concept can also be used to test machine-learning interatomic potentials, whose reliability near diffusion transition states still requires validation, as explored here for methane with UMA. More broadly, the results establish uptake-rate measurements as a practical, trend-level benchmark for molecular diffusion models in narrow-pore zeolites, particularly when direct diffusion measurements are inaccessible or uncertain.

Acknowledgements
We acknowledge the financial support from the Czech Science Foundation under project No. 25-16013S. Computational resources were provided by e-INFRA CZ (ID: 90254).

Funding
This work was supported by the Czech Science Foundation (project No. 25-16013S). Computational resources were provided by e-INFRA CZ (ID: 90254).

Author contributions
T.V. performed the molecular dynamics simulations and DFT calculations; J.H. carried out the hydrocarbon mass transport measurements and sample characterization; Y.G. synthesized the Si-CHA sample; R.B. supervised the experimental work; R.B. and O.B. wrote the main manuscript text. All authors reviewed the manuscript.

Data availability
The datasets generated and analyzed during the current study (raw uptake curves, simulation input files, and force-field parameters) are available in the Zenodo repository, https://doi.org/10.5281/zenodo.23337707. All other data supporting the findings of this study are included in this published article and its Supplementary Information files.

Additional information
Competing interests: R.B. is an Editorial Board Member of Scientific Reports. The other authors declare no competing interests.

References

(1) Feliczak-Guzik, A. Hierarchical zeolites: Synthesis and catalytic properties. *Microporous and Mesoporous Materials* **2018**, *259*, 33–45.
(2) Saab, R.; Polychronopoulou, K.; Zheng, L.; Kumar, S.; Schiffer, A. Synthesis and performance evaluation of hydrocracking catalysts: A review. *Journal of Industrial and Engineering Chemistry* **2020**, *89*, 83–103.

(3) Peng, J.; Wang, H.; Olson, D. H.; Li, Z.; Li, J. Efficient kinetic separation of propene and propane using two microporous metal organic frameworks. *Chemical Communications* **2017**, *53* (67), 9332–9335.
(4) Pérez-Botella, E.; Valencia, S.; Rey, F. Zeolites in Adsorption Processes: State of the Art and Future Prospects. *Chemical Reviews* **2022**, *122* (24), 17647–17695.
(5) Li, J.-R.; Kuppler, R. J.; Zhou, H.-C. Selective gas adsorption and separation in metal–organic frameworks. *Chemical Society Reviews* **2009**, *38* (5), 1477–1504.
(6) Medveď, I.; Černý, R. Surface diffusion in porous media: A critical review. *Microporous and Mesoporous Materials* **2011**, *142* (2), 405–422.
(7) Olsbye, U.; Svelle, S.; Bjørgen, M.; Beato, P.; Janssens, T. V.; Joensen, F.; Bordiga, S.; Lillerud, K. P. Conversion of methanol to hydrocarbons: how zeolite cavity and pore size controls product selectivity. *Angew Chem Int Ed Engl* **2012**, *51* (24), 5810–5831.
(8) Awati, R. V.; Ravikovitch, P. I.; Sholl, D. S. Efficient and Accurate Methods for Characterizing Effects of Framework Flexibility on Molecular Diffusion in Zeolites: CH4 Diffusion in Eight Member Ring Zeolites. *The Journal of Physical Chemistry C* **2013**, *117* (26), 13462–13473.
(9) Tagliabue, M.; Farrusseng, D.; Valencia, S.; Aguado, S.; Ravon, U.; Rizzo, C.; Corma, A.; Mirodatos, C. Natural gas treating by selective adsorption: Material science and chemical engineering interplay. *Chemical Engineering Journal* **2009**, *155* (3), 553–566.
(10) Cnudde, P.; Redekop, E. A.; Dai, W.; Porcaro, N. G.; Waroquier, M.; Bordiga, S.; Hunger, M.; Li, L.; Olsbye, U.; Van Speybroeck, V. Experimental and Theoretical Evidence for the Promotional Effect of Acid Sites on the Diffusion of Alkenes through Small-Pore Zeolites. *Angewandte Chemie International Edition* **2021**, *60* (18), 10016–10022.
(11) Khalighi, M.; Chen, Y. F.; Farooq, S.; Karimi, I. A.; Jiang, J. W. Propylene/Propane Separation Using SiCHA. *Industrial & Engineering Chemistry Research* **2013**, *52* (10), 3877–3892.
(12) Zhu, W.; Kapteijn, F.; A. Moulijn, J. Shape selectivity in the adsorption of propane/propene on the all-silica DD3R. *Chemical Communications* **1999**, (24), 2453–2454.
(13) Olson, D. H.; Yang, X.; Camblor, M. A. ITQ-12: A Zeolite Having Temperature Dependent Adsorption Selectivity and Potential for Propene Separation. *The Journal of Physical Chemistry B* **2004**, *108* (30), 11044–11048.
(14) Olson, D. H.; Camblor, M. A.; Villaescusa, L. A.; Kuehl, G. H. Light hydrocarbon sorption properties of pure silica Si-CHA and ITQ-3 and high silica ZSM-58. *Microporous and Mesoporous Materials* **2004**, *67* (1), 27–33.
(15) Trachta, M.; Volný, T.; Rubeš, M.; Bulánek, R.; Bludský, O. QM-MM Approach to the Accurate Description of Slow Diffusion in Porous Materials. *The Journal of Physical Chemistry C* **2023**, *127* (18), 8856–8863.
(16) Porter, A. J.; McHugh, S. L.; Omojola, T.; Silverwood, I. P.; O'Malley, A. J. The effect of Si/Al ratio on local and nanoscale water diffusion in H-ZSM-5: A quasielastic neutron scattering and molecular dynamics simulation study. *Microporous and Mesoporous Materials* **2023**, *348*, 112391.
(17) Kärger, J.; Ruthven, D. M.; Valiullin, R. Diffusion in nanopores: inspecting the grounds. *Adsorption* **2020**, *27* (3), 267–281.
(18) Kärger, J.; Ruthven, D. M.; Theodorou, D. N. *Diffusion in nanoporous materials*; Wiley Online Library, 2012.
(19) Kärger, J.; Vasenkov, S. Quantitation of diffusion in zeolite catalysts. *Microporous and Mesoporous Materials* **2005**, *85* (3), 195–206.
(20) Chmelik, C.; Kärger, J. Imaging of transient guest profiles in nanoporous host materials: a new experimental technique to study intra-crystalline diffusion. *Adsorption* **2010**, *16* (6), 515–523.
(21) Peng, S.; Xie, Y.; Wang, L.; Liu, W.; Li, H.; Xu, Z.; Ye, M.; Liu, Z. Exploring the Influence of Inter- and Intra-crystal Diversity of Surface Barriers in Zeolites on Mass Transport by Using Super-Resolution Microimaging of Time-Resolved Guest Profiles. *Angewandte Chemie International Edition* **2022**, *61* (30), e202203903.

(22) Ghysels, A.; Moors, S. L. C.; Hemelsoet, K.; De Wispelaere, K.; Waroquier, M.; Sastre, G.; Van Speybroeck, V. Shape-Selective Diffusion of Olefins in 8-Ring Solid Acid Microporous Zeolites. *The Journal of Physical Chemistry C* **2015**, *119* (41), 23721–23734.
(23) Trachta, M.; Rubeš, M.; Bludský, O. Toward accurate ab initio modeling of siliceous zeolite structures. *The Journal of Chemical Physics* **2022**, *156* (9).
(24) Dubbeldam, D.; Beerdsen, E.; Vlugt, T. J. H.; Smit, B. Molecular simulation of loading-dependent diffusion in nanoporous materials using extended dynamically corrected transition state theory. *The Journal of Chemical Physics* **2005**, *122* (22).
(25) Xiong, H.; Liu, Z.; Chen, X.; Wang, H.; Qian, W.; Zhang, C.; Zheng, A.; Wei, F. In situ imaging of the sorption-induced subcell topological flexibility of a rigid zeolite framework. *Science* **2022**, *376* (6592), 491–496.
(26) O'Malley, A. J.; Catlow, C. R. A. Molecular dynamics simulations of longer n-alkanes in silicalite: a comparison of framework and hydrocarbon models. *Physical Chemistry Chemical Physics* **2013**, *15* (43), 19024–19030.
(27) Ghojavand, S.; Dib, E.; Mintova, S. Flexibility in zeolites: origin, limits, and evaluation. *Chemical Science* **2023**, *14* (44), 12430–12446.
(28) Wang, J.-Y.; Mangano, E.; Brandani, S.; Ruthven, D. M. A review of common practices in gravimetric and volumetric adsorption kinetic experiments. *Adsorption* **2021**, *27* (3), 295–318.
(29) Yucel, H.; Ruthven, D. M. Diffusion in 4A zeolite. Study of the effect of crystal size. *Journal of the Chemical Society, Faraday Transactions 1: Physical Chemistry in Condensed Phases* **1980**, *76* (0), 60–70.
(30) Kärger, J.; Valiullin, R.; Brandani, S.; Caro, J.; Chmelik, C.; Chmelka, B. F.; Coppens, M.-O.; Farooq, S.; Freude, D.; Jobic, H.; et al. Diffusion in nanoporous materials with special consideration of the measurement of determining parameters (IUPAC Technical Report). *Pure and Applied Chemistry* **2025**, *97* (1), 1–89.
(31) Kočiřík, M.; Struve, P.; Bülow, M. Analytical solution of simultaneous mass and heat transfer in zeolite crystals under constant-volume/variable-pressure conditions. *Journal of the Chemical Society, Faraday Transactions 1: Physical Chemistry in Condensed Phases* **1984**, *80* (8), 2167–2174.
(32) Gao, M.; Li, H.; Yang, M.; Gao, S.; Wu, P.; Tian, P.; Xu, S.; Ye, M.; Liu, Z. Direct quantification of surface barriers for mass transfer in nanoporous crystalline materials. *Communications Chemistry* **2019**, *2* (1), 43.
(33) Díaz-Cabañas, M.-J.; A. Barrett, P. Synthesis and structure of pure SiO2 chabazite: the SiO2 polymorph with the lowest framework density. *Chemical Communications* **1998**, (17), 1881–1882.
(34) Miyamoto, M.; Nakatani, T.; Fujioka, Y.; Yogo, K. Verified synthesis of pure silica CHA-type zeolite in fluoride media. *Microporous and Mesoporous Materials* **2015**, *206*, 67–74.
(35) Schröder, K.-P.; Sauer, J.; Leslie, M.; Richard, C.; Catlow, A.; Thomas, J. M. Bridging hydroxyl groups in zeolitic catalysts: a computer simulation of their structure, vibrational properties and acidity in protonated faujasites (H□Y zeolites). *Chemical Physics Letters* **1992**, *188* (3), 320–325.
(36) Emami, F. S.; Puddu, V.; Berry, R. J.; Varshney, V.; Patwardhan, S. V.; Perry, C. C.; Heinz, H. Force Field and a Surface Model Database for Silica to Simulate Interfacial Properties in Atomic Resolution. *Chemistry of Materials* **2014**, *26* (8), 2647–2658.
(37) Martin, M. G.; Siepmann, J. I. Transferable Potentials for Phase Equilibria. 1. United-Atom Description of n-Alkanes. *The Journal of Physical Chemistry B* **1998**, *102* (14), 2569–2577.
(38) Wick, C. D.; Martin, M. G.; Siepmann, J. I. Transferable Potentials for Phase Equilibria. 4. United-Atom Description of Linear and Branched Alkenes and Alkylbenzenes. *The Journal of Physical Chemistry B* **2000**, *104* (33), 8008–8016.
(39) Bai, P.; Tsapatsis, M.; Siepmann, J. I. TraPPE-zeo: Transferable Potentials for Phase Equilibria Force Field for All-Silica Zeolites. *The Journal of Physical Chemistry C* **2013**, *117* (46), 24375–24387.

(40) Thompson, A. P.; Aktulga, H. M.; Berger, R.; Bolintineanu, D. S.; Brown, W. M.; Crozier, P. S.; in 't Veld, P. J.; Kohlmeyer, A.; Moore, S. G.; Nguyen, T. D.; et al. LAMMPS - a flexible simulation tool for particle-based materials modeling at the atomic, meso, and continuum scales. *Computer Physics Communications* **2022**, *271*, 108171.
(41) Kresse, G.; Furthmüller, J. Efficient iterative schemes for ab initio total-energy calculations using a plane-wave basis set. *Physical Review B* **1996**, *54* (16), 11169–11186.
(42) Blöchl, P. E. Projector augmented-wave method. *Physical Review B* **1994**, *50* (24), 17953–17979.
(43) Grimme, S. Semiempirical GGA-type density functional constructed with a long-range dispersion correction. *Journal of Computational Chemistry* **2006**, *27* (15), 1787–1799.
(44) Perdew, J. P.; Ruzsinszky, A.; Csonka, G. I.; Vydrov, O. A.; Scuseria, G. E.; Constantin, L. A.; Zhou, X.; Burke, K. Restoring the Density-Gradient Expansion for Exchange in Solids and Surfaces. *Physical Review Letters* **2008**, *100* (13), 136406.
(45) Baerlocher, C.; McCusker, L. B.; Olson, B.; Meier, W. M.; International Zeolite Association. Structure, C. *Atlas of zeolite framework types*; Published on behalf of the Structure Commission of the International Zeolite Association by Elsevier, 2007.
(46) Tribello, G. A.; Bonomi, M.; Branduardi, D.; Camilloni, C.; Bussi, G. PLUMED 2: New feathers for an old bird. *Computer Physics Communications* **2014**, *185* (2), 604–613.
(47) Sheppard, D.; Terrell, R.; Henkelman, G. Optimization methods for finding minimum energy paths. *The Journal of Chemical Physics* **2008**, *128* (13).
(48) García-Sánchez, A.; Dubbeldam, D.; Calero, S. Modeling Adsorption and Self-Diffusion of Methane in LTA Zeolites: The Influence of Framework Flexibility. *The Journal of Physical Chemistry C* **2010**, *114* (35), 15068–15074.
(49) Halamek, J.; Volný, T.; Bulánek, R.; Blahut, J.; Čejka, J.; Eliášová, P.; Opanasenko, M.; Bludský, O. Defect-induced channel blockage drives propene and propane separation in PCR zeolites. *Chemical Engineering Journal Advances* **2026**, *26*, 101229.
(50) Wood, B. M.; Dzamba, M.; Fu, X.; Gao, M.; Shuaibi, M.; Barroso-Luque, L.; Abdelmaqsoud, K.; Gharakhanyan, V.; Kitchin, J. R.; Levine, D. S.; et al. UMA: A Family of Universal Models for Atoms. 2026.

Supplementary Files

This is a list of supplementary files associated with this preprint. Click to download.

- SIfinalrev2.pdf